Int. J. Heat Mass Transfer. Vol. 31, No. 10, pp. 2123–2135, 1988
Printed in Great Britain

0017–9310/88 $3.00 + 0.00

Natural convection suppression in horizontal annuli by azimuthal baffles

H. Q. YANG and K. T. YANG
Department of Aerospace and Mechanical Engineering, University of Notre Dame, Notre Dame, IN 46556, U.S.A.

and

J. R. LLOYD
Department of Mechanical Engineering, Michigan State University, East Lansing, MI 48824, U.S.A.

(*Received* 23 *December* 1987 *and in final form* 24 *March* 1988)

Abstract—Numerical computations based on the control volume approach using orthogonal coordinates are carried out for conjugate natural convection within a horizontal cylindrical annulus. The purpose is to study the possible suppression of convection by azimuthal baffles. The baffles are placed at the top, central and bottom regions of the annular gap. The Rayleigh number based on the annular gap width is varied from 1.0×10^2 to 10^6 for radius ratios of 4.0 and 1.4. The fluid is air, and the transport properties depend on temperature. The most efficient way of reducing heat transfer is the case where the baffle prevents direct flow onto the inner and outer cylinders. When the baffle is at the position where the crescent-shaped streamlines are stretched, an increase of heat transfer occurs. Only a small reduction in heat transfer is obtained when the baffle is placed in the stagnant region of the annulus.

INTRODUCTION

THE STUDY of natural convection in a horizontal annulus has many important applications such as insulation of underground pipe-in-pipe systems, electronic cooling, aircraft cabin insulation, solar collector design, nuclear reactor design, etc. Under certain circumstances, the convection needs to be suppressed in the annulus and thus may become one of the important considerations in the design process. Considerable experimental and numerical studies have been directed towards understanding the physics of the natural convection phenomena in the concentric and eccentric cylindrical annuli. Comprehensive and excellent reviews of the investigations up to 1976 have been given by Kuehn and Goldstein [1, 2] and will not be repeated here. In recent years, studies have been made in the high Rayleigh number range [3, 4], concentric and eccentric annuli with and without rotation [5–10], effect of variable properties [11–14], mixed boundary conditions [15, 16], other physical effects [17–21], three-dimensionality [22–24], density inversion [25, 26], and transient responses [27, 28].

Farouk and Guceri [4] presented numerical solutions for Ra ranging from 10^6 to 10^7 with a K–ε turbulence model and a radius ratio of 2.6. The results showed good agreement with experimental data. Projahn *et al.* [7] used a body-fitted coordinate system to investigate the local and overall heat transfer between concentric and eccentric horizontal cylinders for the following range of parameters, Ra from 10^2 to 10^5, Prandtl number of 0.7, and various eccentric positions of the inner cylinder. The same problem has been studied numerically by Cho *et al.* [8] using a bipolar coordinate system and by Prusa and Yao using a radial transformation. The study by Lee [10] indicated that the rotation of the inner cylinder causes a decrease in Nusselt number throughout the flow for a fixed Rayleigh number. Hessami *et al.* [11], Mahony *et al.* [13] and Bishop and Brandon [14] investigated the effect of variable properties on the natural convection in the horizontal annulus, their findings are almost the same as those in a square enclosure studied by Zhong *et al.* [29]. Basically, the Boussinesq approximation is valid for a temperature difference ratio $(T_H - T_C)/T_C < 0.1$, but can be used for the ratio up to 0.2 with reasonable accuracy in the calculated heat transfer rate. The Boussinesq approximation does overestimate the tangential velocity and temperature gradient near the hot inner cylinder. Kumar [15] presented the numerical results for constant heat flux at the inner cylinder and isothermal condition at the outer cylinder. A lower effective sink temperature is obtained when it is compared to isothermal heating, thus a higher heat transfer rate is expected. Glakpe *et al.* [16] studied a problem similar to the one by Kumar [15], but with a diffuse radiative wall and where vertical variation of eccentric position is taken into account. As emissivity is changed from 0 to 0.6, the heat transfer rate decreases significantly for all Rayleigh numbers investigated. Rao *et al.* [23] investigated numerically and experimentally the natural convective

NOMENCLATURE

a	coefficients in equation (12)
A	area
c_p	isobaric specific heat
c_{pm}	mean specific heat
g	determinant of covariant metric tensor g_{ij}
g^{ij}, g_{ij}	contra-covariant metric tensor
G^i	gravitational acceleration vector, $i = 1, 2, 3$
h_i	scale factor in the direction x^i
J	total heat flux
k	thermal conductivity
k_{eq}	equivalent conductivity
k_{eqi}, k_{eqo}	equivalent conductivity at inner and outer cylinders, respectively
L	length scale, $R_o - R_i$
n^i	normal vector, $i = 1, 2, 3$
Nu	Nusselt number, hL/k
p	static pressure
Pr	Prandtl number
q^i	conduction heat flux in the direction i
Q	heat flux
R	radial coordinate
R_i, R_o	radii of inner and outer cylinders, respectively
RR	radius ratio, R_o/R_i
Ra	Rayleigh number, $\rho g\beta(T_H - T_C)L^3/\mu_R\alpha_R$
T	temperature
u^i	velocity components, $i = 1, 2, 3$
v	volume
x^i	orthogonal coordinates, $i = 1, 2, 3$
Δx^i	incremental dependent variable.

Greek symbols

α	thermal diffusivity
β	volume expansion coefficient
δ_{ij}	Kronecker delta
θ	angular coordinate
μ	dynamic viscosity
ρ	density
σ_t^j	shear stress tensor.

Subscripts

C	cold wall
H	hot wall
i, j, k	coordinate indices
n, s, e, w	nodal designation on the control volume surfaces
P, N, S, E, W	nodal designation of basic grid
R	reference quantities
s	solid
t	time derivative.

flow in horizontal concentric annuli with emphasis on the various flow patterns. By two- and three-dimensional calculations over a range of Ra and radius ratio, the transition to the multicellular flow pattern which has been observed in Powe *et al.*'s experiment [30] is confirmed, and an oscillating flow is generated at the upper part of the annulus as Rayleigh number increases. A similar problem has also been studied by Fusegi and Farouk [24] with a relatively small axial length to show the end effects.

Clearly, most of the investigations so far are for the plain annuli. A few investigations are on annuli with radial spacers [31, 32] or with various transverse fins [33–35]. Kwon *et al.* [31] studied, both theoretically and experimentally, convection in an annulus with three equally spaced axial spacers. A spacer made of material with low thermal conductivity reduces heat transfer by as much as 20%, while the one with high conductivity suppresses the natural convection heat transfer between the cylinders. Good agreement with experimental data on temperature distribution and local heat transfer coefficients were obtained. The experimental study by Babus'Haq *et al.* [32] with eccentric cylinders found a 20% decrease in heat transfer with two low conductivity radial spacers and an 8% increase with a single vertical baffle. The studies by Kwon and co-workers [33, 34] and Tolpadi and Kuehn [35] are about horizontal cylinders in the infinite medium with conducting plate fins and transverse circular fins.

This paper is motivated by an interest in demonstrating the possible suppression of natural convection and reduction of heat transfer in horizontal concentric cylindrical annuli using azimuthal baffles as well as in revealing complex interactions between the baffle and the fluid. Our attention is directed largely to locating the baffles midway between the cylinders (at $(R_o + R_i)/2$), with an arc length subtended by an angle of 90° at several symmetric positions. The baffle positions are shown in Fig. 1. Here, an inner cylinder is heated at a higher temperature T_H, an outer cylinder surface is maintained at a lower temperature T_C. The following cases are considered. In type I (Fig. 1(a)) the azimuthal angle subtended by the baffle is from −45° to 45°; type II (Fig. 1(b)) from 135° to 225°; type III (Fig. 1(c)), a combination of types I and II; type IV (Fig. 1(d)) from 45° to 135°, and from 225° to 315°; and type V (Fig. 1(e)), a combination of types III and IV, or a complete partition. The length scale L is taken as $(R_o - R_i)$, the difference between the radii of the cylinders. The ratio of the thermal conductivity of the baffle material to that of the fluid (at T_C) is 10. The thickness of the baffle is $1/36L$. The Rayleigh number based on L in this study varies from 10^2 to 10^6 for radius ratios (R_o/R_i) of 1.4 and 4.0.

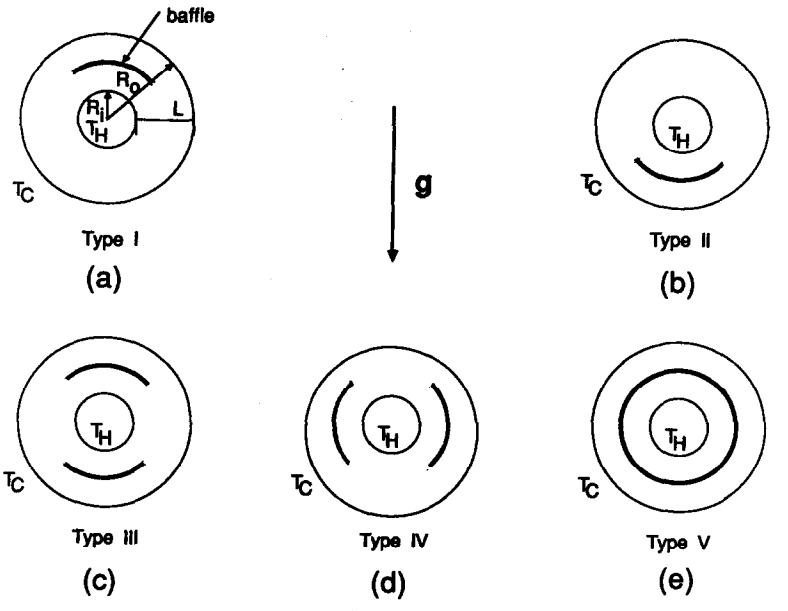

FIG. 1. Geometries of cylindrical annulus with several types of baffles.

The numerical solution procedure is based on primitive variables and the temperature dependence of transport properties is taken into account. The Boussinesq approximation is not invoked. The governing equation is based on the control volume approach using orthogonal coordinates. The results of this study have been validated with experimental and other numerical results available in the literature for the limiting cases of the plain annuli.

GOVERNING EQUATIONS AND SOLUTION PROCEDURE

The equations describing the natural convection phenomena inside an annulus are the conservation equations of mass, momentum and energy. In most previous studies they are written in cylindrical polar coordinates. The equations used in this study are, however, in orthogonal coordinates. The advantage of orthogonal coordinates lies in its generality. Thus complex geometries can be dealt with. Moreover, once the computer code is written, various geometries definable by orthogonal coordinates can be studied by merely changing the scale factors h_i (see below for definition). The computer program used in this paper was originally written for solving the three-dimensional mass, momentum and energy equations in generalized three-dimensional orthogonal coordinates with application to the problem of fire spread in a confined pressure vessel [36]. The success of the code in simulating the natural convection in three-dimensional confined enclosures has been demonstrated in ref. [37]. The present computation, however, is carried out for the two-dimensional flow since the three-dimensional effects exist only near the end walls [24]. Moreover, the two-dimensional calculation requires less CPU time. As a result, the grid can be refined and a better accuracy can be realized.

The governing equations in the Cartesian coordinates in the tensor form have been used in our previous studies. The corresponding equations in the orthogonal coordinates can be obtained using standard tensor transformations as shown in ref. [37]. The equations for the fluid medium then take the following forms:

$$\rho_{,t}+g^{-1/2}(g^{1/2}\rho u^i/h_i)=0 \tag{1}$$

$$(\rho u^i)_{,t}+g^{-1/2}(g^{1/2}\rho u^i u^j/h_j)_{,j}=-p_{,i}/h_i+\rho G^i+g^{-1/2}(g^{1/2}\sigma_i^j/h_j)_{,j}-(h_i)_{,j}/(h_i h_j)(\rho u^i u^j-\sigma_i^j)+(h_j)_{,i}/(h_i h_j)(\rho u^j u^j-\sigma_j^j) \tag{2}$$

$$(\rho c_{pm}T)_{,t}+g^{-1/2}(g^{1/2}\rho c_{pm}u^i T/h_i)_{,i}=-g^{-1/2}(g^{1/2}q^i/h_i)_{,i}. \tag{3}$$

Here ρ is the fluid density, u^i the contravariant component of the velocity vector, g the determinant of covariant metric tensor g_{ij}, h_i the scale factor, p the static pressure, G^i the component of the gravity acceleration vector, σ_i^j the stress tensor, c_{pm} the mean isobaric heat capacity, q_i the conduction heat flux, μ the dynamic viscosity, and subscript t denotes derivatives with respect to time.

It should be noted that the scale factor h_i is for the curvilinear coordinates in the direction i, it is not a component. Therefore, the summation rule does not apply to the index of h_i.

The shear stress tensor is given by

$$\sigma_i^j=\mu[h_j/h_i(u^j/h_j)_{,i}+h_i/h_j(u^i/h_i)_{,j}+2(h_i)_{,k}u^k/(h_j h_k)\delta_i^j-\tfrac{2}{3}g^{-1/2}(g^{1/2}u^k/h_k)_{,k}\delta_i^j] \tag{4}$$

and the conduction heat flux q^i by

$$q^i = -k/h_i T_{,i} \quad (5)$$

here k is the thermal conductivity of the fluid.

The equation governing the energy transport inside the baffles is the heat conduction equation

$$(\rho_s c_{pm} T_s)_t = -g^{-1/2}(g^{1/2} q_s^i/h_i)_{,i}. \quad (6)$$

Here the conduction flux is given by

$$q_s^i = -k_s/h_i (T_s)_{,i}. \quad (7)$$

Subscript s denotes the solid.

The boundary conditions at the cylindrical surfaces are the prescribed temperatures, and the non-slip conditions. At the interface of the baffle and fluid, the compatibility conditions of temperature and heat flux are required

$$T = T_s, \quad q^i n^i = q_s^i n^i \quad (8)$$

or

$$k/h_i (T)_{,i} n^i = k_s/h_i (T_s)_{,i} n^i \quad (9)$$

where n^i is the component of the unit vector normal to the interface.

The control volume approach as described in ref. [37] to solve equations (1)–(3) is utilized. Basically, the conservation equations are first integrated over the control volume of $g^{1/2}\,dx^1\,dx^2$. The convective and diffusive terms can be expressed adequately in terms of the value at the surfaces of the cell, a procedure similar to the one in the Cartesian coordinates as described by Patankar [38]. The difference lies in the fact that the surface area is allowed to change from point to point. The tensor terms due to the curvature of the coordinates are averaged in the cell. For example, equation (3) will become, after integration

$$(\rho c_{pm} T)_t \Delta v + J_e^1 A_e - J_w^1 A_w + J_n^2 A_n - J_s^2 A_s = 0. \quad (10)$$

Here J is the total heat flux due to convection and conduction, A the area $(h_i \Delta x^i h_j \Delta x^j)$, v the volume, and subscripts e, w, n and s denote the point at which it is to be evaluated, as shown in Fig. 2. Thus

$$J^1 = \rho c_{pm} u^1 T - q^1. \quad (11)$$

The approximation to the convective term $\rho c_{pm} u^1 T$ is by the QUICK scheme, and conduction terms by central difference as utilized in our previous studies [39, 40].

The finite difference equations can be finally written as

$$a_P T_P = a_E T_E + a_W T_W + a_N T_N + a_S T_S. \quad (12)$$

The solution procedure of equation (12) follows the standard tridiagonal matrix solver algorithm.

The treatment of conduction equation (6) inside baffles is somewhat similar. After integrating equation (6), the same form as equation (10) is obtained, but with

$$J^1 = -q_s^1. \quad (13)$$

By imposing zero velocity inside the baffles, one can reduce expression (11) to equation (13) at the interfaces, so that the heat flux compatibility condition can be automatically satisfied, when the conduction equation (6) is grouped into equation (3). For the momentum equations, an analogous finite difference equation, equation (12), can be formed, but with T replaced by u^1 or u^2. When baffles are to be considered, modifications are to be made in terms of a's, so that the velocities inside the baffles are always zero.

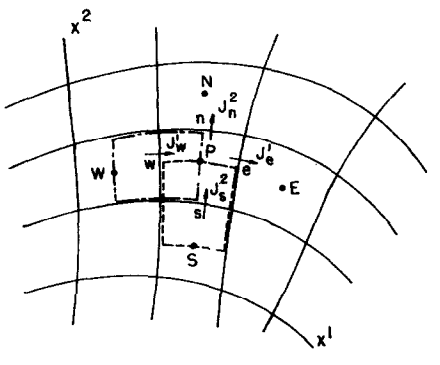

FIG. 2. Orthogonal control volume and nodal points.

RESULTS AND DISCUSSIONS

Initial solutions are obtained first for the unobstructed annulus case, so that direct comparison with published results can be made. After validating the program with published results, computations for cases with baffles are then performed.

Accuracy of the numerical solutions

From the symmetry of the problem, clearly, only half the cylinder needs to be considered. Validation studies of the present solution algorithm and the code have been performed by generating a solution which can be compared directly with previously published results. The results for the case of $RR = 2.6$ and $Ra = 4.7 \times 10^4$ studied by Kuehn and Goldstein [1] using air were considered, since other investigators have also used their data for validation. The transport properties of the fluid (air) are allowed to vary with temperature. The density of air is evaluated from the equation of state, and other properties are taken from those in ref. [41], namely

$$c_p = 0.2383 - 0.7915 \times 10^{-5} T + 0.4834 \times 10^{-7} T^2 \ \text{kJ kg}^{-1}\,\text{K}^{-1} \quad (14)$$

$$\mu = (14.58 \times 10^{-5} T^{3/2})/(110.4 + T) \ \text{kg s}^{-1}\,\text{m}^{-1} \quad (15)$$

$$k = (2.6482 \times 10^{-6} T^{1/2})/(1 + 245.4 \times 10^{(-12/T)}/T) \ \text{W m}^{-1}\,\text{K}^{-1}. \quad (16)$$

As for the present study, T_C is fixed at 288.15 K, and the dimensionless temperature ratio $(T_H - T_C)/T_C$ is taken to be 0.2, which is the threshold value for the

validity of the Boussinesq approximation [13]. The computations have been carried out on an IBM 3033 mainframe. The CPU time required generally depends on the problem. For example, at a Rayleigh number of 10^4 and $RR = 2.6$, approximately 2 h of CPU time is required to reach convergent and steady-state solution. For higher Rayleigh numbers, more CPU time is required. The results are presented in terms of streamlines, isotherms, flow patterns, local and overall heat transfer rates. Since the geometry differs from that of a rectangular enclosure, an equivalent conductivity k_{eq} is introduced to account for variation of areas in the inner and outer cylinders. Here the equivalent conductivity is taken to be the ratio of heat flux due to convection and conduction to that due to conduction alone in the plain annulus case

$$k_{eq} = Q_{conv+cond}/Q_{cond}. \tag{17}$$

It can be evaluated locally and globally at the inner and outer cylinders. The equivalent conductivity k_{eq} can be interpreted as the thermal conductivity that a motionless fluid in the gap would have to transmit the same amount of heat as the moving fluid. It can be taken as an equivalent Nusselt number for the cylinder geometry as well.

Shown in Fig. 3 is the variation of local equivalent conductivity at the inner and outer cylinders (k_{eqi} and k_{eqo}) with azimuthal angle by the present computations, and that by Kuehn and Goldstein [1] obtained experimentally by interferometry and by numerical calculations. The radial dimensionless temperature distribution at various azimuthal angles are also compared. This is shown in Fig. 4 for 30°, 90° and 150°. The present calculations for all three angles compare well with the experimental data [1]. Listed in Table 1 are the overall equivalent conductivities by several other investigators. The overall comparisons are good. Furthermore, the balance of energy at the inner and outer surface and across each concentric cylindrical surface has been checked. The general errors are found to be less than 1.0%.

Grid refinement studies have also been carried out by several sets of uniform meshes at $Ra = 10^5$, $RR = 2.6$. The results for the 30×36 grid presented in this paper are compared with the corresponding results of 24×20 and 48×40 grids, as displayed in Fig. 5 which shows the variation of the local k_{eq} with azimuthal angle for different mesh numbers. The mesh number of 30×36 ($r \times \theta$) is found to be optimum in terms of computer effort and accuracy. The overall k_{eq} for 20×24 is 3.5119, 3.4481 for 30×36, and 3.4330 for 48×40. The difference between the results for grids of 36×30 and 48×40 is thus less than 0.5%.

The overall Nusselt number k_{eq} for various Rayleigh numbers is given in Fig. 6. Several other previously published results are also shown for comparison. For $RR = 2.6$ the present results are compared with the experimental data of Kuehn and Goldstein [1]; for $RR = 4.0$ compared with that of Lee [10] with $RR = 5.0$; and $RR = 1.4$ compared with that of the correlation curve given by Raithby and Hollands [42]. The agreement is again excellent.

Baffle locations for types I, II *and* III

Before discussing the possible reduction of heat transfer by baffles, it is desirable to examine the energy transfer process in an unobstructed cylindrical annulus. Isotherms (right) and streamlines (left) for the case of $RR = 4.0$ and $Ra = 10^5$, and a dimensionless temperature difference ratio of 0.2 are shown in Fig. 7(a). For this high Rayleigh number, the boundary layer is well defined along the inner cylinder, and the flow consists of two crescent-shaped convective cells, symmetric with respect to the vertical central line. The fluid immediately adjacent to the warm inner cylinder rises due to the buoyant force with a corresponding increase in the boundary layer thickness. At the top of the inner cylinder the thermal boundary layer

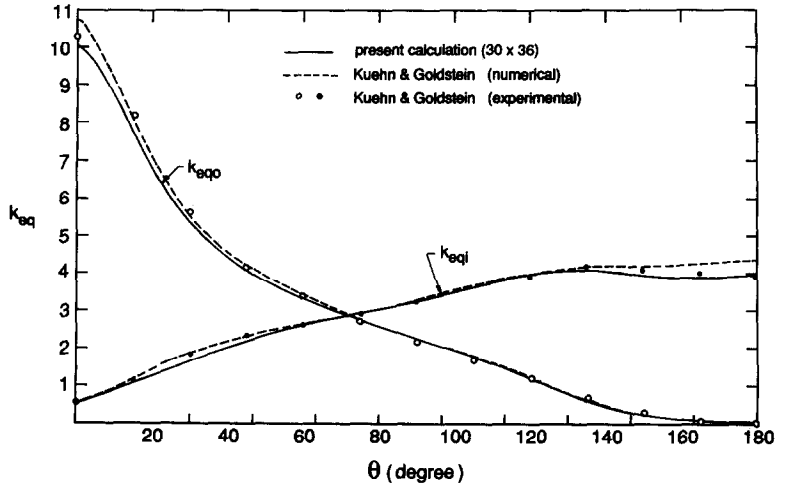

FIG. 3. Comparison of local equivalent conductivity k_{eq} distribution at inner and outer cylinders at $Ra = 4.7 \times 10^4$, $Pr = 0.71$ and $RR = 2.6$.

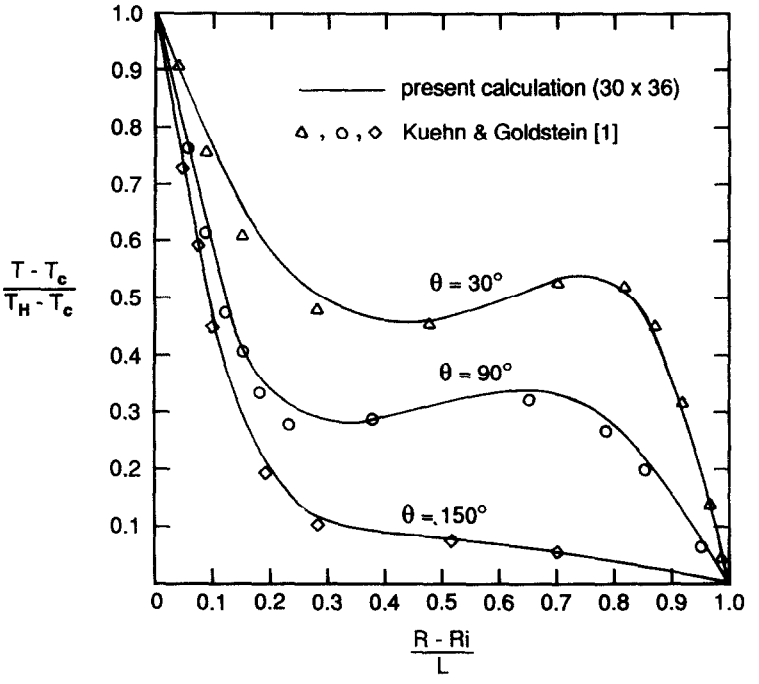

FIG. 4. Comparison of temperature distributions for different angular positions at $Ra = 4.7 \times 10^4$, $Pr = 0.71$ and $RR = 2.6$.

around it and also the flow separate, forming a thermal plume. The hot upflowing of fluid impinges on the cold outer cylinder surface at $\theta = 0°$, and is cooled. The fluid descends along the outer cylinder toward the bottom of the annulus. As the fluid approaches the bottom at $\theta = 180°$, it encounters an adverse pressure gradient which forces it to separate away from the outer cylinder and move to the bottom of the inner cylinder. As a result of the impinging hot fluid, the local heat transfer rate near the region is expected to be high. This can clearly be observed in Fig. 7(a) from the dense isotherms near the top of the outer cylinder, and from the distribution of k_{eqo} in Fig. 8. Since flow separation occurs at the bottom of the outer cylinder near 180° and at the top of the inner cylinder, minimum heat transfer is observed in these locations. Hence, the key to the success in reducing heat transfer lies in blocking direct impingement of the fluid. The study of the cylindrical annulus with internal baffles of types I, II, III is carried out for this purpose.

Figure 7(b) shows the streamlines (left) and isotherms (right) with baffle type I. In this case, a single azimuthal baffle is inserted symmetrically at the top of the inner cylinder. The fluid still flows up along the inner cylinder forming a boundary layer and separates near the top of it. Due to the presence of the baffle, the thermal plume is distorted before being fully developed. At the interface between the baffle and the fluid, energy exchange occurs, which results in a heat transfer from the fluid below the baffle to the fluid at the top of the baffle. This can be visualized through the isotherms passing through the baffle. Heated by the warm fluid, the baffle maintains a temperature higher than that of the outer cylinder, so that a second cell is generated on the top of the baffle.

Table 1. Comparison of overall heat transfer rate for air at $RR = 2.6$

	Kuehn and Goldstein [1]		Hessami *et al.* [11]	Present
	Exp.	Num.	Num.	Num.
Ra	4.7×10^4	5.0×10^4	5.0×10^4	4.7×10^4
k_{eqi}	3.0	3.024	3.26	2.943
k_{eqo}	3.0	2.973	3.05	2.901

By comparing the isotherms in Fig. 7(a) with those in Fig. 7(b), one sees that the isotherms near the outer cylinder at $\theta = 0°$, where the maximum local heat flux occurs in the plain cylinder case, becomes less dense in the presence of the baffle. This is a result of the decreased strength of the impinging fluid, which is obvious from the peak value of the stream function of the second cell in Fig. 7(b) at the top of the baffle. At an angle near 60° the isotherms become more dense since part of the hot fluid impinges on the region after being deflected from the tip of the baffle. However, it is not as dense as that at $\theta = 0°$ for the plain cylinder case (Fig. 7(a)). Since the fluid does not have enough distance to accelerate, the resulting flow is less vigorous. The temperature inversion at the center of the annulus for the plain cylinder case is replaced by stratified isotherms representing a slow core flow region.

From the streamline of Fig. 7(b), it is obvious that flow still separates near the top of the inner cylinder, but due to the presence of the baffle, it has to turn over along the baffle surface. At the tip of the baffle,

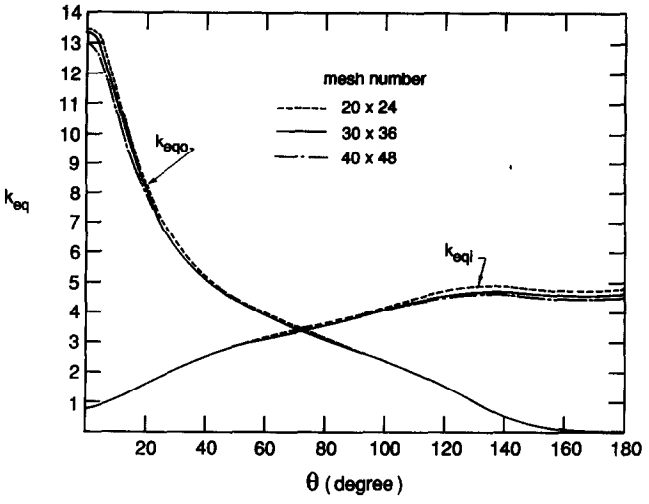

FIG. 5. Local k_{eq} distribution at different grid mesh numbers for an unobstructed annulus at $Ra = 10^5$, $Pr = 0.71$ and $RR = 2.6$.

separation occurs with part of the fluid climbing along the baffle due to the buoyancy force. The rest is deflected off the baffle tip and directed toward the outer cylinder due to inertia. This fluid then flows to the bottom, completing the circulation. Comparing streamlines in Fig. 7(a) with those in Fig. 7(b), the point which corresponds to the maximum stream function value is pushed to the central region, and the stagnant region at the bottom of the annulus has been squeezed. The flow pattern is no longer a crescent. It is interesting to note the local heat transfer distributions along the inner and outer cylinders as shown in Fig. 8(a). The local maximum heat transfer is greatly reduced in the region for $\theta = 0°$–$45°$ due to the insertion of the baffle. This effect is due to the fact that the hot fluid is prevented from directly impinging on the cooled surface. However, the level of heat transfer is still high due to the generation of the second cell at the top of the baffle. The quantity k_{eqo} at $\theta > 45°$ has a local minimum and maximum. The minimum is from the separation of the second cell and the main cell, while the maximum is a result of flow separation at the edge of the baffle. As a result of the heat balance from the inner to the outer cylinders, the reduction in k_{eqi} is expected. Actually, the reduction in k_{eqi} can be seen in the figure throughout the range of 0°–140°. The overall heat transfer in this case is reduced by 16%.

When the baffle is placed at the bottom of the inner cylinder as type II, the isotherms of Figs. 7(a) and (c) differ very little. This is because the bottom part of the plain cylinder has a stagnant region. This region of small convection corresponds to the thermally stable fluid between two flat plates, of which the top one is warmer. As a result, the baffle does not separate the flow but merely pushes the streamlines up a bit. A small reduction in heat transfer rate is seen from the local k_{eqo} and k_{eqi} in Fig. 8. In this case, the total decrease is about 3.3%.

When two baffles are inserted at the same time into the cylindrical annulus as shown in Fig. 1(c), which is a combination of types I and II, the top baffle dominates the reduction of heat transfer of the system. This can be easily seen by comparing the curve of k_{eqo} and k_{eqi} for types I and III in Fig. 8(a). Streamlines however show some differences. In Fig. 7(b) where the top baffle exists, the stagnant bottom part in the flow is filled out by the fluid motion. In Fig. 7(d) the bottom baffle resists the circulation of flow, so that fluid has to flow around the baffle. The flow still fills most of the bottom region. Compared with Fig. 7(c) where only the bottom baffle exists, the ability of the flow to penetrate the stagnant region is enhanced due to the effect of the top baffle.

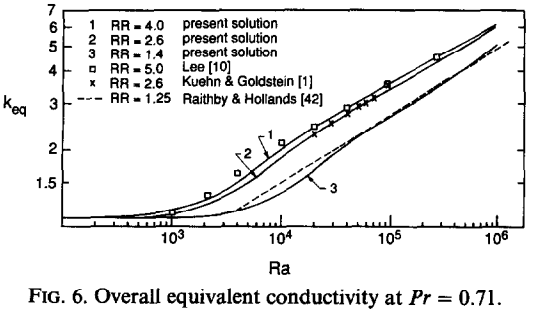

FIG. 6. Overall equivalent conductivity at $Pr = 0.71$.

Baffle location for type IV

When two baffles are symmetrically placed in the central portion of the annulus as shown in Fig. 1(d), interestingly enough, a slight increase instead of a decrease of heat transfer occurs. In Fig. 7(a) where no baffle exists the bottom portion is almost stagnant, and the boundary layer around the inner cylinder is like a cylinder in an infinite medium. There is no direct impinging of the cold fluid on the surface of the inner cylinder near the bottom. However, in Fig. 7(e) where side baffles exist, the streamlines are stretched and the

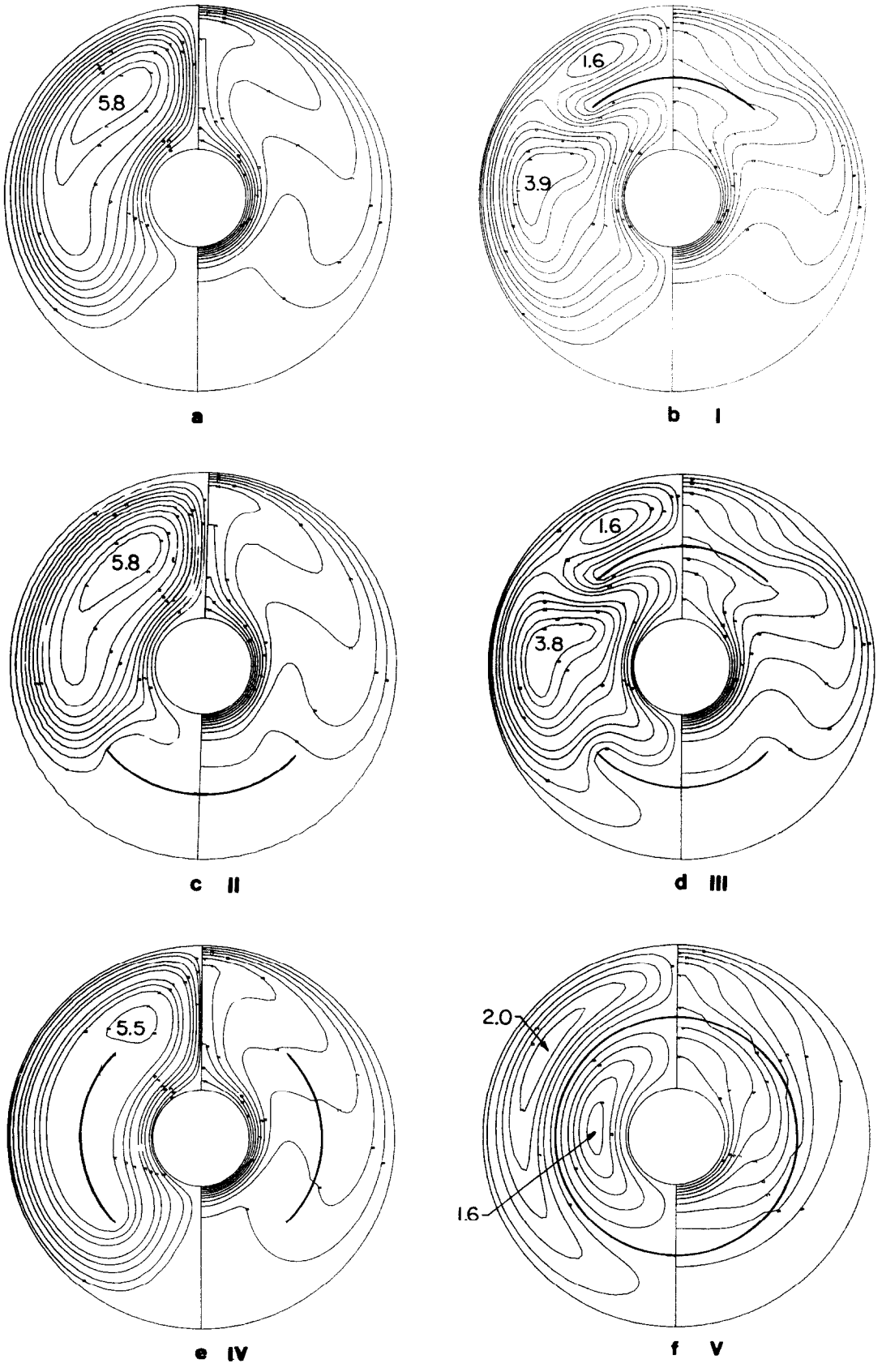

FIG. 7. Streamlines and isotherms for different types of baffle at $Ra = 10^5$ and $RR = 4.0$.

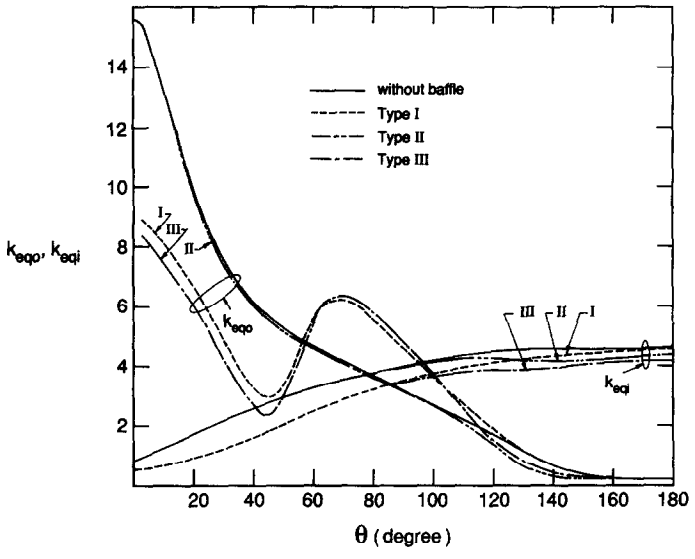

FIG. 8. (a) Local k_{eq} variation with azimuthal angle for types I, II and III at $Ra = 10^5$ and $RR = 4.0$. (b) Local k_{eq} variation with azimuthal angle for types IV and V at $Ra = 10^5$ and $RR = 4.0$.

fluid flows around the baffle from outside. This causes an increase in heat transfer near the bottom at $\theta = 180°$. As for the outer cylinder, the point where separation begins is close to 180° due to the presence of the baffle. Obviously heat transfer to the solid surface is increased. This phenomenon can clearly be observed from the local k_{eq} on the inner and outer cylinder in Fig. 8(b). This effect is not that significant in the central portion due to weak convection in that region as seen from Fig. 7(a). The effect is more pronounced at the edge of the baffle on k_{eqo} and at the bottom on k_{eqi}. In this case, overall heat transfer is increased by almost 2%. The baffle enhances the flow circulation instead of retarding it. It is obvious that the position of the baffle has a very significant influence on the flow.

Baffle location for type V (*whole partition*)

The heat transfer is reduced by as much as 46% when a whole partition is inserted into the cylinders. This decrease can be visualized with the aid of streamlines and temperature contours of Fig. 7(f). A comparison of the peak stream function values in both parts of the annulus indicates that the strength of the flow in either one of the individual parts is less than the non-partitioned annulus. This is to be expected since the partition temperature lies between T_C and T_H, therefore the effective buoyant force in each annu-

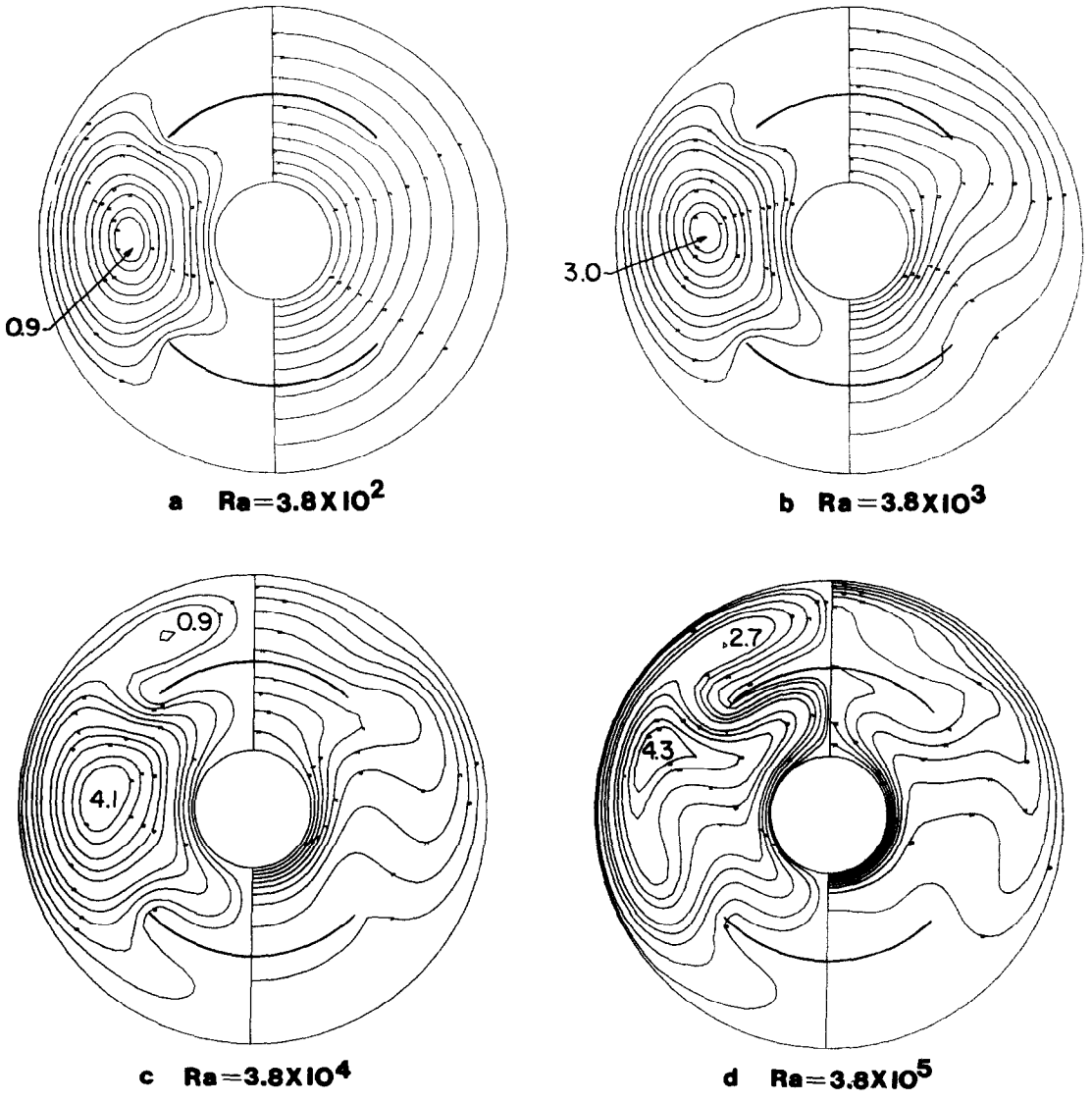

FIG. 9. Streamlines and isotherms for different Rayleigh numbers of type III baffle at $RR = 4.0$.

lus is smaller. At this high Rayleigh number of 10^5, the thermal plume is almost absent. From Fig. 8(b), the local k_{eqo} and k_{eqi} are similarly reduced. Thus the baffle separates flow into two individual regions so that the flow circulation strength and the accompanying convection motion are reduced.

Rayleigh number effects

Figure 9 shows the streamlines and isotherms at several Rayleigh numbers for the baffle of type III. At low *Ra*, conduction is dominant, flow is very weak and only occurs in the central region at about $\theta = 90°$. Most regions above and below the baffle are stagnant. As a result of geometric symmetry of the baffles with respect to the center, the flows are nearly symmetric with the center near 90°. As the Rayleigh number increases, the flow becomes stronger and the center of circulation moves up. The presence of the baffle resists the motion, therefore the penetration of flow into the stagnant region starts in an asymmetric manner with more flow in the upper regions of both baffles. Meanwhile, the fluid at the top is also disturbed, so that convection dominates the heat transfer from the lower portion of the inner cylinder to around 60° of the outer cylinder. At a higher Rayleigh number of 3.8×10^4, the fluid motion is somewhat of the boundary layer type with all fluid flowing along the surface of the cylinder and the baffle. In the central region of the annulus, a stratified stationary core appears. It is seen that the baffle efficiency in reducing heat transfer is decreasing. The variation of the overall average equivalent conductivity with *Ra* at $RR = 4.0$ and 1.4 is shown in Fig. 10.

For baffle I with $R = 1.4$, several isotherms and streamlines are shown in Fig. 11. Compared to the corresponding ones with $RR = 4.0$, one can see that the general flow characteristics are similar, but the regions between baffle and cylinders are more quiescent.

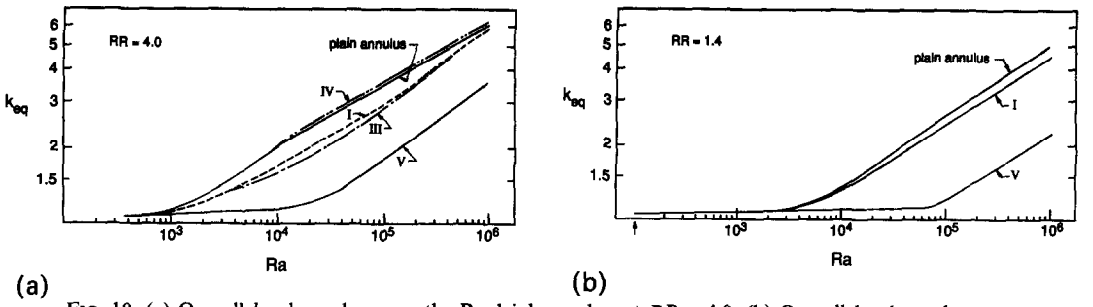

FIG. 10. (a) Overall k_{eq} dependence on the Rayleigh number at $RR = 4.0$. (b) Overall k_{eq} dependence on the Rayleigh number at $RR = 1.4$.

CONCLUDING REMARKS

It should be noted that the baffle thermal conductivity, thickness, radial position and arc length all have certain influences on the results. Our study, nevertheless, is aimed only at providing physical insight to the mechanisms of the suppression of convection. To find the optimal baffle arrangement as well as the best material to use, extensive computations need to be carried out. Radiation may also

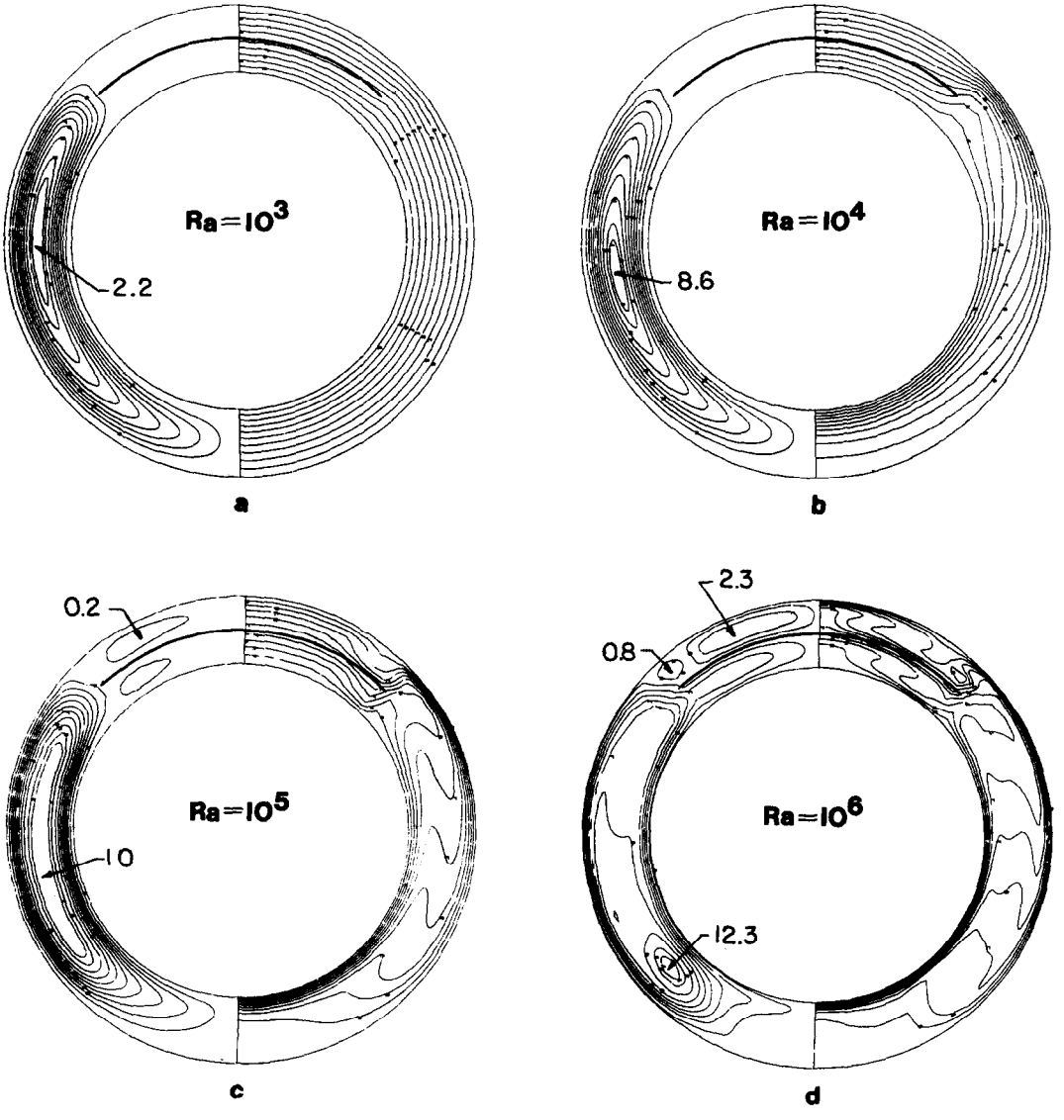

FIG. 11. Streamlines and isotherms for different Rayleigh numbers of type I at $RR = 1.4$.

play an important role in the present problem, but a separate study is needed. In this regard, the analysis and computations in ref. [36] are pertinent.

Acknowledgement—The authors wish to acknowledge the support of the National Science Foundation under Grant CBT82-19158 to the University of Notre Dame.

REFERENCES

1. T. H. Kuehn and R. J. Goldstein, An experimental and theoretical study of natural convection in the annulus between horizontal concentric cylinders, *J. Fluid Mech.* **74,** 695–719 (1976).
2. T. H. Kuehn and R. J. Goldstein, An experimental study of natural convection heat transfer in concentric and eccentric horizontal cylindrical annuli, *J. Heat Transfer* **100,** 635–640 (1978).
3. M. C. Jeschke and M. Farshchi, Boundary layer regime for laminar free convection between horizontal circular cylinders, *J. Heat Transfer* **102,** 228–235 (1980).
4. B. Farouk and S. I. Guceri, Laminar and turbulent natural convection in the annulus between horizontal concentric cylinders, *J. Heat Transfer* **104,** 631–636 (1982).
5. L. S. Yao, Analysis of heat transfer in slightly eccentric annuli, *J. Heat Transfer* **102,** 279–284 (1980).
6. M. Singh and S. C. Rajvanshi, Heat transfer between eccentric rotating cylinders, *J. Heat Transfer* **102,** 347–350 (1980).
7. U. Projahn, H. Rieger and H. Beer, Numerical analysis of laminar natural convection between concentric and eccentric cylinders, *Numer. Heat Transfer* **4,** 131–146 (1981).
8. C. H. Cho, K. S. Chang and K. H. Park, Numerical simulation of natural convection in concentric and eccentric horizontal cylindrical annuli, *J. Heat Transfer* **104,** 624–630 (1982).
9. J. Prusa and L. S. Yao, Natural convection heat transfer between eccentric horizontal cylinders, *J. Heat Transfer* **105,** 108–116 (1983).
10. T. S. Lee, Numerical experiments with laminar fluid convection between concentric and eccentric rotating cylinders, *Numer. Heat Transfer* **7,** 77–87 (1984).
11. M. A. Hessami, A. Pollard and R. D. Rowe, Numerical calculations of natural convection heat transfer between horizontal concentric isothermal cylinders—effects of variation of fluid properties, *J. Heat Transfer* **106,** 668–671 (1984).
12. P. Vasseur, L. Robillard and B. Chandra Shekar, Natural convection heat transfer of water within a horizontal cylindrical annulus with density inversion effects, *J. Heat Transfer* **105,** 117–123 (1983).
13. D. N. Mahony, R. Kumar and E. H. Bishop, Numerical investigation of variable property effects on laminar natural convection of gases between two horizontal isothermal concentric cylinders, *J. Heat Transfer* **108,** 783–795 (1986).
14. E. H. Bishop and S. C. Brandon, Heat transfer by natural convection of gases between horizontal isothermal concentric cylinders: the expansion number effect, *Proc. ASME/JSME Thermal Engng Joint Conf.*, Vol. 2, pp. 275–280 (1987).
15. R. Kumar, Numerical study of natural convection in a horizontal annulus with constant heat flux on the inner wall, *Proc. ASME/JSME Thermal Engng Joint Conf.*, Vol. 2, pp. 187–193 (1987).
16. E. K. Glakpe, C. B. Watkins, Jr. and J. N. Cannon, Laminar natural convection between concentric and eccentric horizontal cylinders with mixed boundary conditions and radiation, *Proc. ASME/JSME Thermal Engng Joint Conf.*, Vol. 2, pp. 227–233 (1987).
17. S. R. M. Gardiner and R. H. Sabersky, Heat transfer in annular gap, *Int. J. Heat Mass Transfer* **21,** 1459–1466 (1978).
18. L. S. Yao and F. F. Chen, Effects of natural convection in the melted region around a heated horizontal cylinder, *J. Heat Transfer* **102,** 667–672 (1980).
19. T. H. Kuehn and R. J. Goldstein, A parametric study of Prandtl number and diameter ratio effects on natural convection heat transfer in horizontal cylindrical annuli, *J. Heat Transfer* **102,** 768–770 (1980).
20. M. C. Charrier-Mojtabi, A. Mojtabi and J. P. Caltagirone, Numerical solution of a flow due to natural convection in horizontal cylindrical annulus, *J. Heat Transfer* **101,** 171–173 (1979).
21. M. A. Hessami, A. Pollard, R. D. Rowe and D. W. Ruth, A study of free convective heat transfer in a horizontal annulus with a large radii ratio, *J. Heat Transfer* **107,** 603–610 (1985).
22. Y. Takata, K. Iwashige, K. Fukuda and S. Hasegawa, Three-dimensional natural convection in an inclined cylindrical annulus, *Int. J. Heat Mass Transfer* **27,** 747–754 (1984).
23. Y. Rao, Y. Miki, K. Fukuda and Y. Takata, Flow patterns of natural convection in horizontal cylindrical annuli, *Int. J. Heat Mass Transfer* **28,** 705–714 (1985).
24. T. Fusegi and B. Farouk, A three-dimensional study of natural convection in the annulus between horizontal concentric cylinders, *Proc. 8th Int. Heat Transfer Conf.*, San Francisco, Vol. 4, pp. 1575–1580 (1986).
25. T. H. Nguyen, P. Vasseur and L. Robillard, Natural convection of cold water in concentric annular spaces: effect of the maximum density, *Proc. 7th Int. Heat Transfer Conf.*, Vol. 2, pp. 251–256 (1982).
26. T. H. Nguyen, P. Vasseur and L. Robillard, Natural convection between horizontal concentric cylinders with density inversion of water for low Rayleigh numbers, *Int. J. Heat Mass Transfer* **26,** 1559–1568 (1983).
27. E. Van De Sande and B. J. G. Hamer, Steady and transient natural convection in enclosures between horizontal circular cylinders (constant heat flux), *Int. J. Heat Mass Transfer* **22,** 361–370 (1979).
28. Y. T. Sui and B. Tremblay, On transient natural convection heat transfer in the annulus between concentric, horizontal cylinders with isothermal surfaces, *Int. J. Heat Mass Transfer* **27,** 103–111 (1984).
29. Z. Y. Zhong, K. T. Yang and J. R. Lloyd, Variable property effects in laminar natural convection in a square enclosure, *J. Heat Transfer* **107,** 133–138 (1985).
30. R. E. Powe, C. T. Carley and E. H. Bishop, Free convective flow patterns in cylindrical annuli, *J. Heat Transfer* **91,** 310–314 (1969).
31. S. S. Kwon, T. H. Kuehn and T. S. Lee, Natural convection in the annulus between horizontal circular cylinders with three axial spacers, *J. Heat Transfer* **104,** 118–124 (1982).
32. R. F. Babus'Haq, S. D. Probert and M. J. Shilston, Influence of baffles upon natural-convective steady-state heat transfers across horizontal air-filled annuli, *Proc. 8th Int. Heat Transfer Conf.*, San Francisco, Vol. 4, pp. 1557–1561 (1986).
33. S. S. Kwon and T. H. Kuehn, Conjugate natural convection heat transfer from a horizontal cylinder with a long vertical longitudinal fin, *Numer. Heat Transfer* **6,** 85–102 (1983).
34. S. S. Kwon, T. H. Kuehn and A. K. Tolpadi, On natural convection from a short conducting plate fin below a heat horizontal cylinder, *J. Heat Transfer* **106,** 661–664 (1984).
35. A. K. Tolpadi and T. H. Kuehn, Numerical study of three-dimensional natural convection from a horizontal cylinder with transverse circular fins, *Proc. 8th Int. Heat Transfer Conf.*, San Francisco, Vol. 3, pp. 1305–1310 (1986).
36. J. Raycraft, M. D. Kelleher, H. Q. Yang and K. T. Yang,

Fire spread in a three-dimensional pressure vessel with radiation exchange and wall heat losses, Technical Report 88-NFS-3, Department of Aerospace and Mechanical Engineering, University of Notre Dame, Notre Dame, Indiana (May 1988).
37. H. Q. Yang, K. T. Yang and J. R. Lloyd, A numerical study of three-dimensional laminar natural convection in a horizontal cylinder with differentially-heated end walls at high Rayleigh numbers, *Proc. Symp. Heat and Mass Transfer in Honor of Professor B. T. Chao*, University of Illinois at Urbana-Champaign, pp. 153–195 (1987).
38. S. V. Patankar, *Numerical Heat Transfer and Fluid Flow*. Hemisphere, Washington, DC (1980).
39. H. Q. Yang, K. T. Yang and J. R. Lloyd, Flow transition in laminar flow in a three-dimensional tilted rectangular enclosure, *Proc. 8th Int. Heat Transfer Conf.*, San Francisco, Vol. 4, pp. 1495–1500 (1986).
40. H. Q. Yang, K. T. Yang and J. R. Lloyd, Laminar natural convection flow transition in tilted three-dimensional longitudinal rectangular enclosures, *Int. J. Heat Mass Transfer* **30**, 1637–1644 (1987).
41. H. Hilsenrath, *Table of Thermodynamics and Transport Properties of Air, Argon, Carbon Dioxide, Hydrogen, Oxygen, and Steam*. Pergamon Press, New York (1960).
42. G. D. Raithby and K. G. T. Hollands, A general method of obtaining approximate solution to laminar and turbulent convection problems. In *Advances in Heat Transfer* (Edited by T. F. Irvine and J. P. Hartnett), Vol. 11, pp. 265–325. Academic Press, New York (1975).

SUPPRESSION DE LA CONVECTION NATURELLE DANS UN ESPACE ANNULAIRE HORIZONTAL PAR DES BAFFLES AZIMUTAUX

Résumé—Des calculs numériques basés sur la méthode du volume de contrôle et des coordonnées orthogonales sont conduits pour traiter la convection naturelle conjuguée dans un espace annulaire cylindrique et horizontal. Le but est d'étudier la possibilité d'annuler la convection par des baffles azimutaux. Ceux-ci sont placés au sommet, dans le centre et en bas. Le nombre de Rayleigh basé sur la largeur d'espace annulaire varie entre 10^2 et 10^6 pour des rapports de rayons de 4,0 et 1,4. Le fluide est l'air dont les propriétés dépendent de la température. Le moyen le plus efficace pour réduire le transfert thermique est d'empêcher l'écoulement direct de la paroi interne à la paroi externe. Quand le baffle est à une position qui favorise les lignes de courant en forme de croissant, on constate un accroissement du transfert de chaleur. On obtient seulement une faible réduction du transfert quand le baffle est placé dans la zone morte de l'espace annulaire.

UNTERDRÜCKUNG DER NATÜRLICHEN KONVEKTION IN HORIZONTALEN RINGRÄUMEN DURCH SEITLICH ANGEBRACHTE BLECHE

Zusammenfassung—Mit Hilfe von Kontroll-Volumina werden numerische Berechnungen mit orthogonalen Koordinaten für konjugierte natürliche Konvektion in einem horizontalen zylindrischen Ringraum durchgeführt. Das Ziel der Untersuchungen ist eine mögliche Unterdrückung der Konvektion durch seitliche Bleche. Die Bleche sind oben, in der Mitte und unten in dem ringförmigen Zwischenraum angebracht. Die Rayleigh-Zahl (mit der Spaltbreite des Ringzwischenraums als charakteristischer Länge) wird von 10^2 bis 10^6 für die Radienverhältnisse von 4,0 und 1,4 variiert. Das verwendete Fluid ist Luft, dessen Stoffeigenschaften temperaturabhängig sind. Der effizientere Weg zur Reduzierung des Wärmetransports ist der Fall, wo die Bleche die direkte Strömung auf den inneren und den äußeren Zylinder verhindern. Der Wärmeübergang wird verbessert, wenn die Bleche an der Stelle angebracht sind, wo die halbmondförmigen Stromlinien gestreckt werden. Nur eine geringe Verminderung des Wärmeübergangs tritt auf, wenn die Bleche im Stagnationsgebiet des Ringraumes angebracht sind.

ПОДАВЛЕНИЕ ЕСТЕСТВЕННОЙ КОНВЕКЦИИ В ГОРИЗОНТАЛЬНЫХ КОЛЬЦЕВЫХ КАНАЛАХ С ПОМОЩЬЮ АЗИМУТАЛЬНЫХ ПЕРЕГОРОДОК

Аннотация—Сопряженная естественная конвекция внутри горизонтального кольцевого канала исследуется численно методом контрольного объема с использованием ортогональных координат. Цель исследования—изучить возможность подавления конвекции с помощью азимутальных перегородок, которые размещены в верхней, центральной и нижней областях кольцевого канала. Число Рэлея, основанное на величине зазора, изменялось в диапазоне $1{,}0 \times 10^2$–10^6 для отношений радиусов 4,0 и 1,4. Рабочей жидкостью служил воздух; учитывалась зависимость переносных свойств от температуры. Наиболее эффективный способ снижения теплопереноса—это размещение перегородки таким образом, чтобы она препятствовала прямому натеканию потока на внутренний и внешний цилиндры. Если перегородка располагалась в центральной части серповидных линий тока, происходило усиление теплопереноса. Когда перегородка находилась в застойной зоне канала, отмечалось только небольшое уменьшение теплового потока.